Cell Membrane Capsules for Encapsulation of Chemotherapeutic and Cancer Cell Targeting *in Vivo*

Li-Hua Peng,[†,§] Yuan-Hong Zhang,[‡,§] Li-Jie Han,[‡] Chen-Zhen Zhang,[†] Jia-He Wu,[†] Xia-Rong Wang,[†] Jian-Qing Gao,*,[†] and Zheng-Wei Mao*,[‡]

[†]Institute of Pharmaceutics, College of Pharmaceutical Sciences, Zhejiang University, Hangzhou 310027, People's Republic of China

[‡]MOE Key Laboratory of Macromolecular Synthesis and Functionalization, Department of Polymer Science and Engineering, Zhejiang University, Hangzhou 310027, People's Republic of China

S *Supporting Information*

ABSTRACT: Systemic administration of chemotherapeutic agents can cause indiscriminate drug distribution and severe toxicity. Until now, encapsulation and targeting of drugs have typically relied on synthetic vehicles, which cannot minimize the clearance by the renal system and may also increase the risk of chemical side effects. Cell membrane capsules (CMCs) provide a generic and far more natural approach to the challenges of drug encapsulation and delivery *in vivo*. Here aptamer AS1411, which can recognize and bind overexpressed nucleolin on a cancer cell membrane, was chemically conjugated onto CMCs. As a result, AS1411 modified CMCs showed enhanced ingestion in certain cancer cells *in vitro* and accumulation in mouse cancer xenografts *in vivo*. Chemotherapeutics and contrast agents with therapeutically significant concentrations can be packaged into CMCs by reversible permeating their plasma membranes. The systematic administration of cancer targeting CMCs loaded with doxorubicin hydrochloride can significantly inhibit tumor growth in mouse xenografts, with significantly reduced toxicity compared to free drug. These findings suggest that cancer targeting CMCs may have considerable benefits in drug delivery and cancer treatment.

KEYWORDS: cell membrane capsules, reversible permeating, targeting, drug delivery, cancer treatment
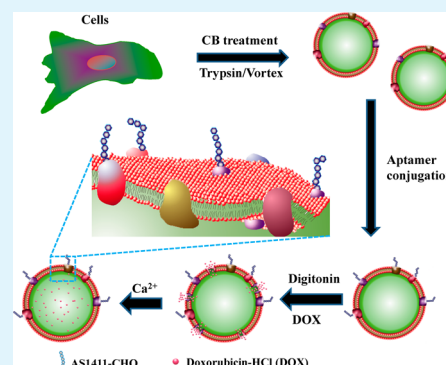
1. INTRODUCTION

Severe toxicity is a major challenge limiting cancer chemotherapy. Lack of cancer cell specificity, indiscriminate drug distribution and rapid clearance necessitate frequent administration of high doses of chemotherapeutics to get a satisfactory clinical response.[1] Synthetic nanoparticles (10−100 nm in diameter), such as phospholipid liposomes,[2,3] amphiphilic molecular micelles,[4,5] polymersomes,[6] polymer nanospheres,[7−10] to name a few, can encapsulate the cytotoxic drug in a vehicle and target it to cancer cells, finally leading to an improved pharmacokinetic efficiency and therapeutic efficacy. Nonetheless, these artificial carriers are usually recognized by our defense system inside the body possibly due to the non-natural surface characteristics in terms of chemistry, morphology and mechanics, and subsequently resulted in fast clearance and toxic immune reactions.[11] Notwithstanding these defects, the development of advanced synthetic drug carriers is currently vigorously pursued. Among them, the "biomimetic camouflage" strategies are gaining popularity based on the concept of "learning from nature".[12] Erythrocyte ghosts,[13] vesicles derived from bacteria,[14,15] virus-like particles,[16,17] targeted protocells[18] and cell membrane coated nano/microparticles[19−21] have been proposed as potential strategies for developing next generation drug carriers. However, another direction, which is often overlooked, is the existence and efficacy of natural counterparts to these artificial carriers.

In response to various stimuli, cells are capable of changing their cytoskeleton structure and encapsulating cytosolic elements by plasma membrane movement, leading to the generation of cell membrane capsules (vesicles). These vesicles not only contain messenger molecules, enzymes and even genes but also are capable of transferring these bioactive molecules from one cell to another.[22,23] Recently, Tang et al. successfully demonstrated that cell membrane vesicles, derived from apoptotic tumor cells, can package and deliver chemotherapeutic drugs, leading to tumor inhibition.[24] However, the use of apoptotic cells still raises the concerns of safety issues and fast clearance inside the body. Therefore, it is of paramount importance to develop an efficient and safe method to prepare cell membrane vesicles from healthy human cells.

To address this important challenge, novel cell membrane capsules (CMCs) from mouse fibroblasts and human embryonic kidney cells were prepared using cytochalasin B (CB), a drug that reversibly affects cytoskeleton membrane interaction.[25,26] These CMCs maintained the entire cell

membrane structure composed of cell membrane lipids and proteins, which also exhibited important membrane functions such as selective permeability and the potential to avoid the attack from macrophages *in vitro*.[26] However, it will be necessary to load therapeutic agents into CMCs at relative high concentration and navigate them to specific tissues or cells *in vivo*. This will require an easy and effective way to introduce targeting moieties on the surface of CMCs and subsequently change the distribution of CMCs *in vivo*. Besides, CMCs could only encapsulate some special cell membrane permeable fluorescent probes in a previous study.[26] It still requires establishment of a general way to load CMCs with cell membrane impermeable and toxic therapeutics, such as hydrophilic chemotherapeutics, where conventional methods are not valid due to the well ordered structure of the cell membrane and limited permeability.

In this study, targeting of CMCs toward cancer cells *in vitro* and mouse tumor xenografts *in vivo* is achieved via conjugation of aptamer AS1411 recognizing overexpressed nucleolin on the cancer cell membrane. Drug and contrast agent are encapsulated into CMCs by reversibly permeating their plasma membranes (Figure 1). Consequently, significant tumor growth
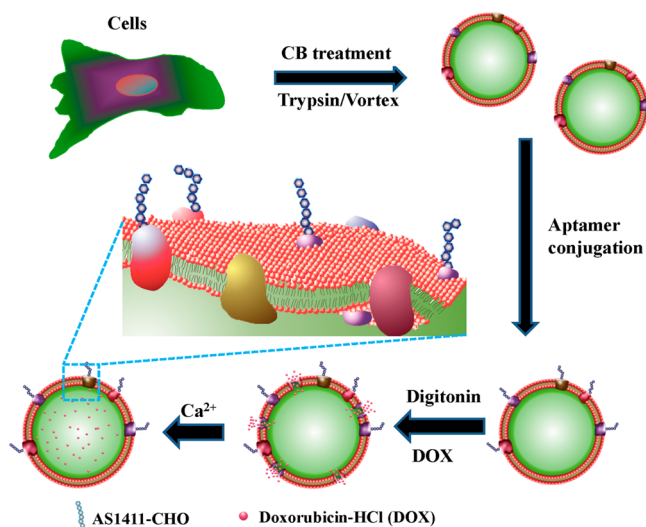
Figure 1. Schematic illustration of the preparation process of functional cell membrane capsules (CMCs). The process can be divided into four steps: deriving CMCs from cells, surface modification with aptamer AS1411, load antitumor drug by reversible permeating plasma membrane and reseal cell membrane by addition of Ca^{2+} ions.

inhibition with remarkably reduced toxicity compared to free drug is achieved by systematic administration of cancer cells targeting CMCs loaded with doxorubicin.

2. EXPERIMENTAL DETAILS

2.1. Materials. Cytochalasin B, carboxyfluorescein diacetate-succinimidyl ester (CFDA-SE), calcein-AM, 3-(4,5-dimethylthiazol-2-yl)-2,5-diphenyltetrazolium bromide (MTT), dimethyl sulfoxide (DMSO), gadolinium-diethylenetriamine pentaacetic acid (Gd-DTPA) and 4′,6-diamidino-2-phenylindole (DAPI) were purchased from Sigma-Aldrich. Triton X, CM-Dil and BCA (bicinchoninic acid) detection kit were purchased from Beyotime Co., Ltd. (Wuhan, China). Indocyanine Green was purchased from TCI, Japan. The sequence of AS1411 is 5′-(GGTGGTGGTGGTTGTGGTGG-TGGTGG). Aptamers fluorescein-AS1411-CHO and AS1411-CHO were purchased from Sangon Biotech Co., Ltd. (Shanghai, China). Doxorubicin hydrochloride (DOX) was purchased from Zhejiang

Hisun Pharmaceutical Co., Ltd. (China). All other chemicals were of analytical grade and used without further purification. Milli-Q water was used throughout the experiments.

2.2. Preparation of CMCs. Endothelial cells are located at the inner wall of blood vessels with good blood compatibility, making them good candidates to generate CMCs. Human endothelial cells (CRL-1730) were obtained from the American Type Culture Collection (ATCC, USA). Cells were maintained in high-glucose RPMI 1640 medium (Gibco) supplemented with 100 U/mL penicillin, 100 μg/mL gentamicin and 10% heat-incativated fetal calf serum (FCS, Gibco). Cells were incubated at 37 °C in a humidified atmosphere containing 5% CO_2 and used at 90% of confluence. To produce CMCs, cells were cultured in a 75 cm^2 flask until 90% confluence, washed twice with PBS and then incubated in 2 mL of serum free RPMI-1640 containing 10 μg/mL Cytochalasin B for 30 min at 37 °C. The cells and formed CMCs were detached by incubation with PBS containing 0.25% trypsin and 0.01% EDTA at 37 °C for 5 min. The cells/CMCs suspension was transferred into a 15 mL centrifuge tube and vigorously shaken for 60 s, and was mixed with the same volume of FCS to obtain a final FCS concentration of 50%. The mixture was centrifuged twice at 1000 rpm for 5 min to remove cells and larger CMCs aggregates. The supernatant was centrifuged again at 4000 rpm for 15 min to collect the CMCs. The CMCs were redispersed and stored in PBS/50%FCS solution containing 10% DMSO at −20 °C. The fluorescent labeled cells were obtained after incubation with 10 μg/mL CFDA-SE, which is a widely used cell-labeling agent, in serum free medium for 1 h and following 24 h in normal medium. Fluorescent CMCs then can be prepared from these cells.

2.3. Characterization of CMCs. The sizes of the CMCs were measured at room temperature by dynamic light scattering (DLS) on a Brookhaven particle size analyzer (90plus). The ζ-potential measurements were performed using an aqueous dip cell in the automatic mode (Zetasizer 3000, Malvern Instruments, Southborough, MA). All data was averaged from 5 parallel measurements. CMCs were stained in 10 μg/mL CM-Dil, a lipophilic marker intercalates in plasma membrane, in PBS for 15 min at 37 °C. After washed twice by centrifugation at 4000 rpm for 15 min, the CMCs were observed under confocal laser scanning microscopy (CLSM, TCS SP5, Leica). The number and concentration of fluorescent labeled CMCs were counted under CLSM, and their mass was calculated in consideration of the average diameter (930 nm) and the density (1 g/mL). The morphology of CMCs was also observed under transmission electron microscopy (TEM). About 50 million CMCs were collected and fixed for 1 h with 2.5% (v/v) glutaraldehyde. After centrifugation and wash with PBS, the CMCs were postfixed for 1.5 h in 1% (v/v) osmium tetroxide at room temperature. The samples were dehydrated in graded series of ethanol (30, 70, 95 and 100 vol %) and propylene oxide. The samples were then embedded in Durcupan (Fluka, Sigma-Aldrich), where polymerization took place at 60 °C for 48 h. Ultrathin sections with a thickness of about 60 nm were mounted on nickel grids and stained with uranyl acetate before examination under a JEOL JEM1010 microscope.

The mouse leukemic monocyte macrophage cell line Raw264.7 cells were purchased from Cell Bank of Typical Culture Collection of Chinese Academy of Sciences (Shanghai, China), and maintained in cell culture medium consisting of high glucose DMEM, supplemented by 10% FBS, 100 U/mL penicillin and 100 μg/mL streptomycin at 37 °C in a 5% CO_2 humidified incubator. The Raw264.7 cells were seeded at a density of 1×10^4 cells per well in a 96-well plate. After cultured for 16 h, the culture medium was changed with a fresh one containing CMCs of variable concentrations. At determined time intervals, 20 μL of MTT (5 mg/mL in PBS) was added to each well and the cells were incubated at 37 °C for another 3 h. The dark blue formazan crystals generated by the mitochondria dehydrogenase in viable cells were dissolved by dimethyl sulfoxide (DMSO). The absorbance at 570 nm was determined by a microplate reader (Biorad Model 680). Three parallel experiments were carried out, and the data were normalized to that of the CMCs-free control. Secretion of TNF-α and IL-6 of the cultured Raw264.7 cells were measured by enzyme

linked immunosorbent assay (ELISA, Nos. ab46105 and ab100712, Abcam, USA) according to the user manuals, respectively. Each value was averaged from four parallel experiments.

2.4. Surface Conjugation of Aptamer AS1411. The AS1411 aptamer capped with an aldehyde end group (AS1411-CHO) was covalently conjugated CMCs via the coupling reaction between the aldehyde groups and $-NH_2$ groups of membrane proteins of CMCs. Briefly, various amount of AS1411-CHO (or fluorescein-AS1411-CHO) was incubated with 1 mg of CMCs PBS suspension for 4 h at 37 °C. The obtained Apt-CMCs were collected by centrifugation at 4000 rpm for 15 min and washed three times against PBS to remove physically absorbed aptamer molecules. The fluorescein-Apt-CMCs were observed under CLSM.

2.5. Drug Loading and Release in Apt-CMCs. 0.2 mg of Apt-CMCs was incubated in various drug solutions in the presence of digitonin for a determined time period at 37 °C. Then a certain amount of $CaCl_2$ was added into the mixture, and the solution was further incubated for another 2 h at 37 °C. The Apt-CMCs and drug were collected by centrifugation at 4000 rpm for 15 min and washed with PBS three times to remove free drugs. The amount of loaded DOX, dextran and Gd-DPTA in the Apt-CMCs was measured after the Apt-CMCs were completely destroyed in a cell lysis buffer to release encapsulated drug, referring to an established standard curve, respectively. The release profiles of DOX from Apt-CMCs resealed under various Ca^{2+} concentrations were studied at 37 °C in PBS buffer. In a typical experiment, 3 mg of Apt-CMCs/DOX was incubated in 1 mL of PBS at 37 °C and shaken at 500 rpm. At desired time intervals, the suspension was centrifuged at 4000 rpm for 15 min and 0.9 mL of the supernatant was taken out each time from the system, while supplementing the same volume of PBS to keep the total volume constant at 1 mL. The concentration of released DOX was determined by UV−vis spectroscopy. The results were averaged with triple independent experiments.

2.6. Cell Selectivity of Apt-CMCs. The immortalized human normal liver cells (Hepli cells) were kindly donated by Dr. Jun Li from the First Affiliated Hospital, College of Medicine, Zhejiang University. The human liver cancer cells (QGY-7703 cells) were obtained from the Cell Bank of Typical Culture Collection of Chinese Academy of Sciences (Shanghai, China). The Hepli and QGY cells were maintained in low glucose DMEM (Gibco, USA) and high glucose RPMI 1640, respectively. Both culture media were supplemented with 10% FBS, 100 U/mL penicillin and 100 μg/mL gentamicin. The cells were seeded on a 24-well plate at a density of 1×10^5 cells per well and allowed to attach for 16 h. Then they were incubated with 10 μg/mL of CFDA-SE labeled CMCs (their fluorescent intensities have been normalized) for different times. After washed five times with PBS to remove the free CMCs, the cells were detached by trypsin. The uptake amount of the fluorescent CMCs was determined by flowcytometry (FACS Calibur, BD). Cells were gated using forward scatter (FSC) and side scatter (SSC) of an only CMCs control to exclude contaminating free CMCs from the final analysis. All the results were reproduced in three separate experiments.

2.7. Animal Model. 4 to 6 weeks old BALB/c nude male mice, weighing approximately 14 g, and 5 weeks old BALB/c mice, weighing 20 ± 2 g, were obtained from the Shanghai Slaccas Animal Company, China. All animal studies were carried out in accordance with the "Guidelines for Animal Experimentation" by the Institutional Animal Care and Use Committee, Zhejiang University. BALB/c nude mice were quarantined for a minimum of 5 days in the SPF grade Animal House under 12 h light/dark cycles at 24−25 °C with a relative humidity of 50−55%. Tumors were established by subcutaneous (s.c.) injection with QGY-7703 cells (0.1 mL, 3×10^7/mL) in the back of each nude mouse. After solid tumors developed to about 100 mm³ in volume, the mice were used for following experiments.

2.8. *In Vivo* Distribution. The ICG labeled CMCs and Apt-CMCs (40 mg/kg) were injected into nude mice bearing xenograft tumors via tail vein. At predetermined time points (6, 24 and 48 h) postinjection, the mice were sacrificed. Various organs and tissues, including brain, heart, liver, spleen, lung, kidney and tumor, were collected. After

washed with saline, the fluorescent images were detected using a CRi *in vivo* imaging system (CRi, USA).[27]

2.9. Pharmacokinetics Study. BALB/c mice were randomly divided into three groups: (1) DOX solution group, (2) CMC/DOX group and (3) Apt-CMC/DOX group (4 mice per group). The dosage of DOX was 5 mg/kg for all the groups. Drugs were injected into the mice via tail vein (0.2 mL/min). At predetermined time points of 5, 10, 15, 30 min, 1, 2, 4, 8 and 24 h postinjection, blood samples were collected into heparinized polyethylene tubes from the periorbital vein and centrifuged immediately at 6000 rpm for 10 min to obtain plasma. The concentrations of DOX in plasma were assayed by a spectrofluorometric method previously described.[28]

2.10. Tumor Treatment and Characterization. Tumor bearing BALB/c nude mice were randomly separated into six groups: (1) saline group (10 mL/kg), (2) DOX group, (2) CMCs group, (3) Apt-CMCs group, (5) CMC/DOX group and (6) Apt-CMC/DOX group. The dosage of DOX was 5 mg/kg in all the drug containing groups. Each group had eight mice. Drugs were intravenous injected into mice two times per week and continued for five times.

Body weight of the mice and tumor size were measured two times per week, for 3 weeks. Tumor volume was calculated by (length × height × width)/2. Tumors were harvested for further analysis after the mice were euthanized 3 weeks after first drug administration.

The tumors and hearts of mice were cryosectioned to 3 μm at −20 °C and were allowed to air-dry overnight. The samples were then stained with hematoxylin and eosin (H&E) and observed under a light microscope.

Frozen tumor sections (3 μm thick) were fixed with 4% paraformaldehyde. Fluorimetric TUNEL (terminal deoxynucleotidyl transferase (TdT)-mediated dUTP nick-end labeling) staining was performed according to manufacturer's instructions (In Situ Cell Death Detection Kit, Roche, Mannheim, Germany) to investigate the presence of apoptotic cells. In brief, frozen sections were treated with 20 μg/mL proteinase K and then incubated in a nucleotide mixture containing fluorescein-12-dUTP and terminal deoxynucleotidyl transferase (TdT) for 90 min. Positive controls were pretreated with 1 U/mL DNase, and negative controls were incubated without TdT. After that, all sections were counterstained with DAPI. Fluorescence images of apoptotic cells (green), DOX (red) and cell nuclei (blue) were obtained from a Zeiss LSM510 confocal microscope.

The frozen sections of tumors were fixed in cold acetone for 10 min, air-dried for 30 min and treated with 1% H_2O_2 for 10 min at room temperature to eliminate endogenous peroxidases. Samples were rinsed three times (5 min for each time) with PBS, and treated with Powerblock (Biogenex Laboratories, San Ramon, CA) for 6 min to block nonspecific binding. After washed with PBS, the samples were then incubated with anti-CD31 antibody (1:800, BD Biosciences, CA, USA) for 1 h at 37 °C. After three washes with PBS, the samples were treated with secondary biotinylated antirat IgG (1:300, Santa Cruze biotechnology, USA) for 1 h at 37 °C. The slides were washed in PBS and incubated in a 1:50 dilution of avidin−biotinylated enzyme complex (ABC, Vector Laboratories) for 1 h at 37 °C. After three washes with PBS, the samples were treated with substrate chromogen 3-amino-9-ethylcarbazole (Vector Laboratories) for 30 min. The samples were counterstained in 50% Mayer's hematoxylin and coverslipped in glycerin gelatin.

2.11. Statistical Analysis. Data are expressed as mean ± standard deviation (SD). A statistically significant value was set as $p < 0.05$ based on the Student's t test.

3. RESULTS AND DISCUSSION

3.1. Preparation and Characterization of CMCs. Because endothelial cells are located at the inner wall of blood vessels and contact with blood, we expect that these cells have plasma membrane with good blood compatibility, making them good candidates to generate CMCs. Fluorescence microscopy revealed that upon CB treatment, human endothelial cells with the cytoplasm stained by carboxyfluorescein shrank and formed spherical capsules around cells
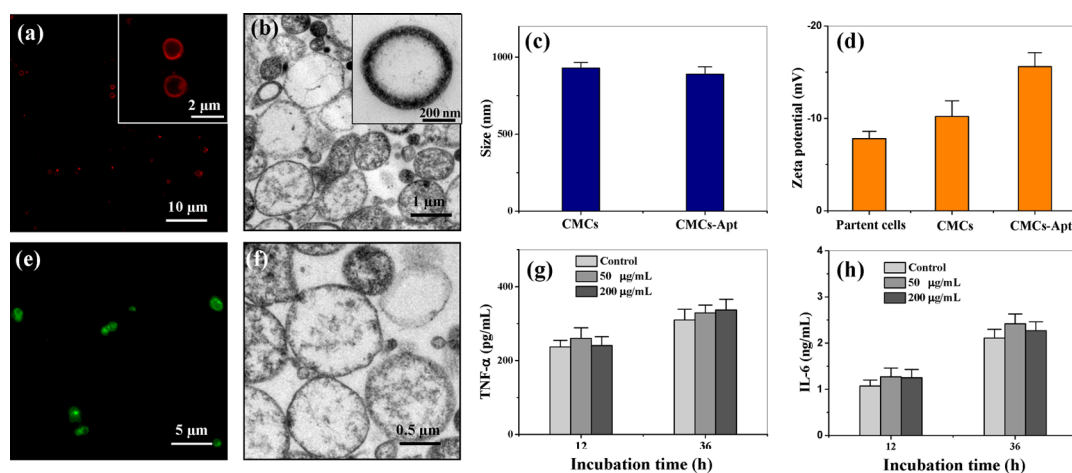
Figure 2. Characterization of the CMCs and the Apt-CMCs. (a) Representative CLSM images of CM-Dil stained CMCs and (b) TEM images of CMCs. Inset shows a high magnification image. (c) Average diameter and (d) surface ζ-potential of CMCs and Apt-CMCs, respectively. (e) CLSM image of fluorescein-Apt-CMCs and (f) TEM image of Apt-CMCs. Secretion of (g) TNF-α and (h) IL-6 of Raw264.7 cells incubated with Apt-CMCs, respectively.
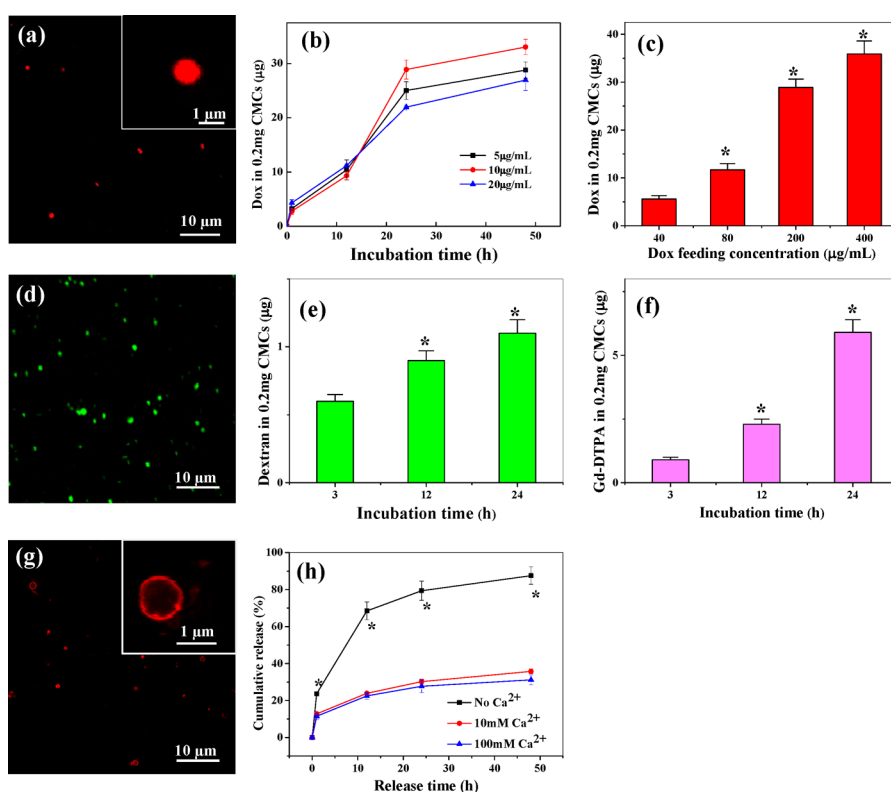
Figure 3. Drug loading and release of the Apt-CMCs. (a) Representative CLSM images of CMCs-Apt loaded with doxorubicin. Inset shows a high magnification image. (b) DOX loading amount in 0.2 mg of CMCs treated with various digitonin solutions as a function of incubation time, where the feeding concentration of DOX is 200 μg/mL. (c) DOX loading amount in 0.2 mg of CMCs for 24 h incubation as a function of DOX feeding concentration. (d) Representative CLSM image of Apt-CMCs encapsulated with FITC labeled dextran. (e) Dextran loading amount in 0.2 mg of CMCs as a function of incubation time, where the feeding concentration of Dextran is 200 μg/mL. (f) Gd-DTPA loading amount in 0.2 mg CMCs as a function of incubation time, where the feeding concentration of Gd-DTPA is 200 μg/mL. (g) Representative CLSM images of CM-Dil stained CMCs undergo digitonin permeating and Ca^{2+} resealing process. (h) The release profile of DOX from Apt-CMCs resealed in different $CaCl_2$ solutions. The * indicates significant difference at the $p < 0.05$ level.

(Figure S1, Supporting Information). The strong green fluorescence of the resultant CMCs indicated the presence of the carboxyfluorescein and thus of cytosolic fluids of the parental cells. These CMCs can be released in the presence of trypsin under mechanical force. CMCs with an average diameter of 930 nm were obtained after several centrifuga-

tion/dispersion cycles to remove larger cells (Figure 2a,c). A single endothelial cell can produce more than 50 CMCs.

The hydrophobic membranes of the resulting CMCs were stained by CM-Dil (Figure 2a), a dye that can bind to the lipid molecules in a cell membrane and emit stable red fluorescence. TEM revealed that the membrane structure of CMCs is intact

and the inner content of the CMCs is cytoplasm (Figure 2b). The integrity of CMCs' membrane was further confirmed by the limited permeability of encapsulated calcein, a hydrophilic fluorescent probe which cannot penetrate hydrophobic cell membrane (Figure S2).

The CMCs possess slightly negative surface charge (Figure 2d), similar to their parental cells, suggesting similar surface characteristics. More importantly, after treated with CB, the majority (over 90%) of the cells are not fluorescent stained by PI/Annexin V assay (Figure S3), suggesting that the cells are not apoptotic or necrotic. The results clearly indicated that the CMCs are not apoptotic bodies.

3.2. Preparation and Characterization of Apt-CMCs.
Oligodeoxynucleotide aptamer AS1411 shows high binding affinity to nucleolin, which is overexpressed on the plasma membrane of some tumor cells.[29,30] Therefore, conjugation of AS1411 onto CMCs will largely enhance their targeting efficiency to specific tumor cells. Given that CMCs membranes preserved certain protein structures with amino groups, conventional conjugation chemistry can be adopted easily to modify the CMCs. In this study, aldehyde group functionalized AS1411 was immobilized on CMCs. Fluorescence microscopy indicated the successful grafting of fluorescein labeled aptamers on the CMCs (Figure 2e). The immobilized amount of AS1411 increased along with its feeding amount and leveled off when the feed amount was higher than 1.0 μg (Figure S4). 0.77 μg of aptamer was conjugated onto 1 mg of CMCs when its feeding amount was 1.0 μg, suggesting the high conjugation efficiency. Taking into account the average particle diameter (~930 nm), this value equaled to 2.9×10^4 molecules per CMC or 2 molecules/10 nm^2. The aptamer conjugation did not significantly influence the membrane structure (Figure 2f) as well as the size and the surface charge of the CMCs (Figure 2c,d).

The *in vitro* toxicity and inflammation of Apt-CMCs was evaluated using mouse leukemic monocyte macrophage Raw264.7 cells. As expected, Apt-CMCs did not have a significant impact on the cell viability at tested concentrations (Figure S5). Moreover, Apt-CMCs did not induce over-expression of inflammatory cytokines such as tumor necrosis factor alpha (TNF-α, Figure 2g) and interleukin-6 (IL-6, Figure 2h) of Raw264.7 cells. All the results suggested that Apt-CMCs are safe carriers without cytotoxicity and will not activate acute inflammation *in vitro*.

3.3. Drug Encapsulation and Sustained Release in Apt-CMCs.
Because CMCs have intact membrane structure and limited permeability, it is quite difficult to load therapeutics that are water-soluble and unable to penetrate into cell plasma membrane by conventional methods. Plasma membranes of cells can be reversibly permeabilized by bacteria toxin Streptolysin O[31,32] or nonionic detergent digitonin.[33−35] A low concentration of digitonin selectively permeabilizes the plasma membrane by complexing with membrane cholesterol.[33] The plasma membrane can be resealed by the addition of Ca^{2+}, by dissociation of the complex of cholesterol and digitonin, leading to an intact membrane again. Then the resealed CMCs can be transferred to normal medium for further application.

The drug loading in digitonin permeabilized Apt-CMCs was evident with both drugs, either by the red autofluorescence of DOX (Figure 3a) or green fluorescence of FITC labeled dextran (Mw 20 kD, Figure 3d). To determine the kinetics of drug packaging, the amount of DOX encapsulated in 0.2 mg of Apt-CMCs in response to varying feeding concentrations of drug or digitonin in the incubation solution or varying incubation time was evaluated. As shown in Figure 3b,c, drug packaging was positively correlated to both the drug feeding concentration and the incubation time. The encapsulated DOX amount rapidly increased along with the incubation time at first 24 h and then the increasing rate slowed down (Figure 3b). The encapsulated DOX amount also rapidly increased along with the feeding concentration (Figure 3c), but the increase speed slowed down when the DOX feeding concentration is higher than 200 μg/mL. The finding of smooth saturable loading kinetics is consistent with a normal or "'Langmuir'" isotherm, suggesting drug diffusion driven by a concentration gradient.[36,37] It is worth noting that the hydrophobic and positively charged nature of DOX may also contribute to the high drug loading efficiency since they may bind and accumulate in the lipid-rich and negatively charged membrane system of CMCs. This hypothesis is evident by the fact that about 8 μg DOX can bind to 200 μg Apt-CMCs by simple coincubation without the presence of digitonin when the DOX concentration is 200 μg/mL (data not shown). The variation of digitonin concentration only brought slight influence on drug encapsulation. At the best case, 28.9 μg of DOX was encapsulated in 200 μg of Apt-CMCs when the DOX feeding concentration was 200 μg/mL. Take the Apt-CMCs with a diameter of 930 nm for example: 480 million Apt-CMCs with weight of about 200 μg. Therefore, each Apt-CMC contains about 0.006 pg of DOX (12.6% of the total weight of CMC/DOX complex), equal to 6 million drug molecules per Apt-CMC.

In contrast, the encapsulation efficiency of dextran into the Apt-CMCs is much lower (Figure 3e): only about 1 μg of dextran was encapsulated in 200 μg of Apt-CMCs. This might be attributed to the significantly larger size of dextran molecules as well as the strong hydrophilicity of the molecules. In addition, we also found that Apt-CMCs could be packaged with contrast agents, such as Gd-DTPA (Figure 3f). This drug loading method is simple and effective.

After resealed by addition of Ca^{2+}, the Apt-CMCs showed an intact membrane structure (Figure 3g). The release of encapsulated DOX is very slow (Figure 3h), especially after the burst release during the first hour (12% of total encapsulated DOX), which might be attributed to the dissociation of adsorbed DOX on membrane. Only another 20% of loaded DOX was further released in the following 47 h, suggesting the low permeability of resealed Apt-CMCs. In contrast, about 70% of the encapsulated DOX was rapidly released in the first 12 h from Apt-CMCs without the resealing process. Besides, the using of digitonin did not bring obvious toxicity to the system (Figure S6). Therefore, the digitonin/Ca^{2+} reversible permeabilization method provides an efficient way to encapsulate therapeutics into CMCs with sustained release profile.

3.4. Cell Targeting of Apt-CMCs *in Vitro*.
Two types of liver-derived cells were used to access the cell selectivity of aptamer tethered CMCs. The QGY-7703 cell is a type of hepatic carcinoma cells that overexpresses nucleolin (the receptor of aptamer AS1411) on the cell membrane. The Hepli cell is a type of immortalized normal liver cells that expresses a normal level of nucleolin on the cell membrane.[30] By comparison, the differences in delivery and uptake of the aptamer-modified CMCs can be distinguished. To make the CMCs detectable via flowcytometry, a cytoplasm staining dye CFDA-SE was preloaded into CMCs.

In general, the normal cells (Hepli) and the cancerous cells (QGY) internalized a relatively small amount of CMCs during the whole experimental period (Figure 4), reaching 8 units of
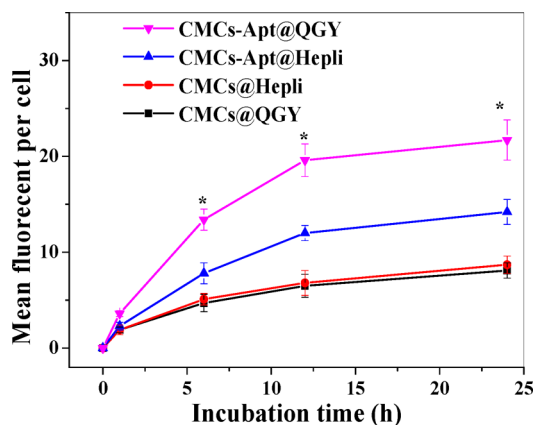

Figure 4. Uptake of CMCs and Apt-CMCs (0.8 μg aptamer per mg CMCs) by QGY-7703 (tumorous) and Hepli (normal) cells as a function of culture time, where the concentration of the CMCs concentration of is 10 μg/mL. The CMCs were stained with CFDA-SE, and their fluorescent intensity was normalized before cell experiments. The * indicates significant difference at the $p < 0.05$ level.

fluorescence after 25 h for both cells, proving that CMCs can effectively minimize recognition and internalization by cells. Hepli cells ingested a little bit more Apt-CMCs, reaching 12 units of fluorescence after 25 h, possibly due to the presence of a certain amount of nucleolin on the surface of normal cells that favor the uptake of AS1411 modified CMCs. In contrast, the QGY cells took up a significantly larger amount of Apt-CMCs (reached 22 units of fluorescence at 25 h, almost 3 time of that of Hepli cells, $p < 0.05$), suggesting the aptamer conjugation can effectively enhance cancer cell recognition and internalization. The internalization of Apt-CMCs was largely inhibited when the nucleolin on cell surface was blocked by free aptamer (Figure S7), proving again the recognition and internalization of Apt-CMCs is attributed to the conjugation of aptamer.

3.5. In Vivo Distribution and Clearance Kinetics of the CMCs. To follow the movement of CMCs inside the animals, indocyanine green (ICG), a water-soluble near-infrared fluorescent dye, was encapsulated into the CMCs by digitonin/Ca^{2+} reversible permeabilization method (9.8 μg ICG in 200 μg CMCs). The in vivo distribution of ICG stained CMCs and Apt-CMCs was studied on nude mice with xenografted tumors generated by QGY liver cancer cells. As shown in Figure 5a, almost no fluorescent signal was found in the organs including brain, heart and spleen within the 72 h after the CMCs or the Apt-CMCs administration, indicating no accumulation of the CMCs or the Apt-CMCs in these organs. In contrast, significant fluorescence was observed in lung and liver tissues in both the CMCs and the Apt-CMCs groups throughout the experimental period, which might be attributed to the relative big size of the CMCs (~930 nm in diameter) and possible denature of their membrane structure during the preparation process and subsequently accumulation in the reticuloendothelial system such as liver and lung.

Despite the residence of the Apt-CMCs in lung and liver tissues, strong fluorescence was also observed in the tumors of the Apt-CMCs group, indicating escape of the Apt-CMCs from the reticuloendothelial system and targeting to the tumor site.
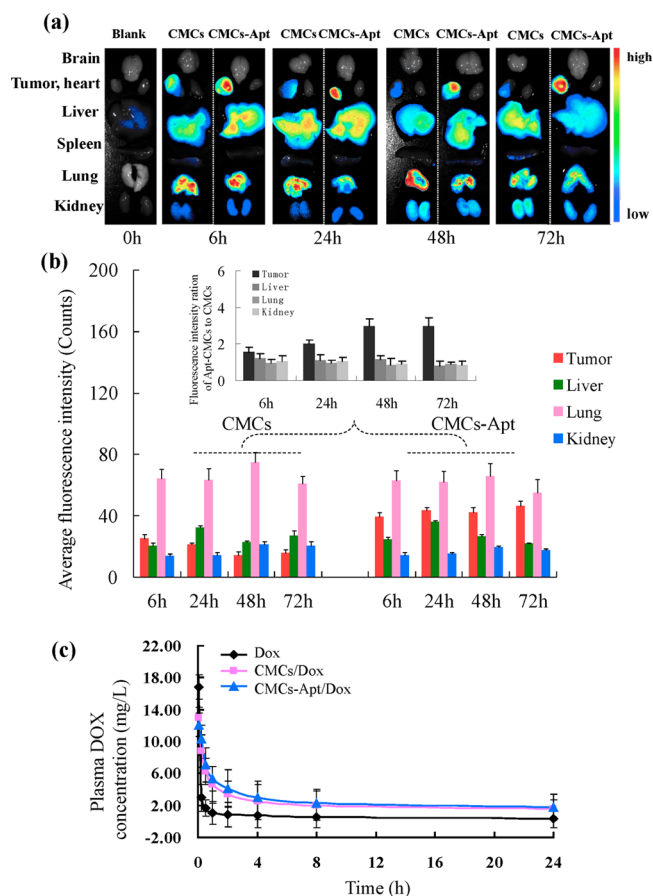
Figure 5. (a) Fluorescent images and (b) normalized fluorescent intensity of different organs from BALB/c nude mice with xenograft tumor, as a function of time postinjection of ICG labeled CMCs and Apt-CMCs, respectively. The ratio of fluorescent intensity in major organs and tumor between Apt-CMCs and CMCs groups is presented as an inset image in panel b. (c) Plasma concentration of DOX in healthy BALB/c mice vs time after administration of free DOX, CMCs/DOX and Apt-CMCs/DOX, respectively.

In contrast, the fluorescence of tumor in CMCs group is much weaker, proving that aptamer immobilization endows tumor targeting ability of the CMCs. The relative fluorescence intensity and the ratio of the Apt-CMCs to the CMCs of major organs were further quantified. As shown in Figure 5b, the concentrations of the CMCs and the Apt-CMCs in lung, liver and kidney tissues are almost the same in the experimental period, indicating the similar distribution pattern and the slow clearance of the CMCs and the Apt-CMCs in major organs. Only the concentration of the Apt-CMCs in tumor is always significantly higher than that of the CMCs, from 1.8-fold (6 h) to 3.1-fold (72 h), should be attributed to the targeting and retention of Apt-CMCs in the tumor site.

The exact mechanism of how these relative large particles escape from the reticuloendothelial system and move to tumor site is still unknown. Nevertheless, a similar phenomenon has also been observed in other cells and cell derived microparticles. For example, mesenchymal stem cells, with a diameter of several to tens of micrometers, can migrate toward and engraft into the sites of tumors, possibly due to chemoattractant signaling, endothelial adhesion, activated infiltration, transmigration and invasion.[38,39] It was reported that intravenously injected BMSCs in mice with xenograft tumor managed to
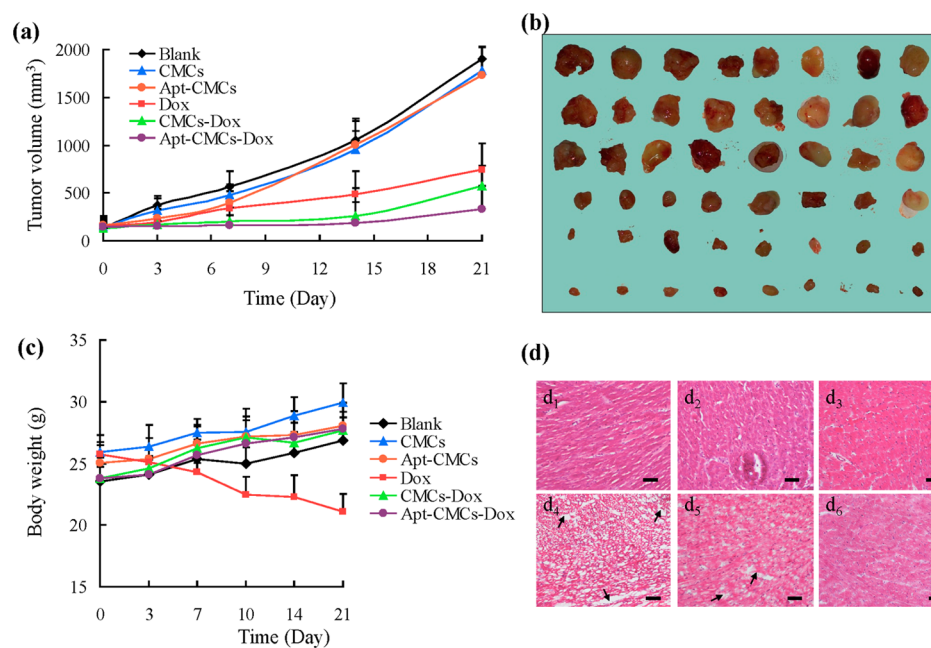
Figure 6. (a) Tumor volume of BALB/c nude mice as a function of culture time after first treatment. (b) Digital images show tumors harvested from mice treated with different groups for 3 weeks (from top to bottom: blank/saline, CMCs, Apt-CMCs, free DOX, CMCs/DOX and Apt-CMCs/DOX groups). (c) Body weight of BALB/c nude mice with xenograft tumors as a function of culture time after first treatment. (d) Optical images of H&E stained heart sections from mice treated with different groups for 3 weeks: (1) saline, (2) CMCs, (3) Apt-CMCs, (4) free DOX, (5) CMCs/DOX and (6) Apt-CMCs/DOX groups. Arrows indicate vacuoles in heart tissues. Scale bar is 50 μm.

home and target the tumor site.[40−43] Furthermore, cell apoptotic microparticles (diameter 0.8−3 μm) also can accumulate in tumor sites after intravenous injection.[24] Thus, we postulate there should be other mechanisms for cells or cell derived particles to escape from the vasculature such as membrane-fusion and active transportation rather than enhanced permeation and retention (EPR) effect, which is widely recognized by small synthetic particles. We shall try our best to conduct a mechanistic study in the future.

To understand the impact of carriers on the clearance kinetics of loaded drug, the blood concentrations of free DOX, CMCs/DOX and Apt-CMCs/DOX were quantatively investigated in healthy mice, respectively. As shown in Figure 5c, following a single IV injection, the free DOX was quickly cleared from the plasma and only <2% of the injected dose remained after 24 h. In contrast, an equivalent dose of DOX encapsulated in the CMCs or the Apt-CMCs displayed remarkably slower clearance profiles, with about 10% of injected dose remained in plasma 24 h postadministration. This could be attributed to the combination of the relatively longer retention time of the CMCs and sustained release of the DOX from the CMCs. DOX encapsulated in the CMCs and the Apt-CMCs showed almost the same pharmacokinetic profiles, indicating the aptamer modification did not influence the circulation behavior of the CMCs. It is worth noting that the centrifugation process used to separate cells from plasma will also remove CMCs and encapsulated DOX, leading to the relatively low plasma concentration of DOX at the beginning.

3.6. In Vivo Cancer Treatment. As shown in Figure 6a, compared to control groups that received intravenous (i.v.) empty CMCs or Apt-CMCs, administration of nontargeted CMCs/DOX (5 mg DOX in 32.8 mg CMCs/kg) to mice with QGY xenografts resulted in highly significant inhibition of tumor growth, especially for the first 2 weeks. This effect is stronger than free DOX, which should be attributed to the long

circulation time of CMCs and sustained release of DOX from CMCs. The tumor-targeted Apt-CMCs/DOX (5 mg DOX in 34.6 mg Apt-CMCs/kg) showed even stronger inhibition of tumor growth, indicates that targeting can significantly enhance drug delivery efficiency. The average volume of tumors from the Apt-CMCs/DOX group after 3 weeks is 333.5 mm^3, significantly smaller than those from the CMCs/DOX group (571.7 mm^3), free DOX group (743.3 mm^3) and drug free control groups (over 1600 mm^3), as shown in Figure 6a,b.

As shown in Figure 6c, the body weight of mice injected with free DOX decreased significantly (18% in 3 weeks, $p < 0.05$), suggesting the systematic toxicity of DOX. Mice treated with empty CMCs or Apt-CMCs and DOX loaded CMCs/DOX or Apt-CMCs/DOX did not show obvious decrease in body weight, indicating good biocompatibility of CMCs and the significantly reduced toxicity of DOX when they were packaged into CMCs.

The most dangerous side effect of DOX is cardiomyopathy, leading to congestive heart failure, due to oxidative stress, downregulation of genes for contractile proteins, and p53 mediated apoptosis.[38] Cardiomyopathy was also found in mice treated with free DOX, illustrated by the appearance of degeneration of myocardial tissue, vacuolization of the cardiomyocytes, and the myofibrillar loss. (Figure 5d). Partial loss of myocardial fibers and the appearance of vacuolated cells also can be found in CMCs/DOX group, although the extent is much lower than that of free DOX group. This might be attributed to the untargeted delivery of CMCs/DOX, leading to relatively high concentration of DOX in heart tissue. By contrast, healthy heart tissues can be observed from other groups, including the APT-CMCs/DOX group, proving again that encapsulation and targeted delivery can significantly reduce the toxicity of DOX.

A close examination of tumor tissues was conducted by H&E staining. As shown in Figure 7a$_1$−a$_3$, robust tumor tissues with
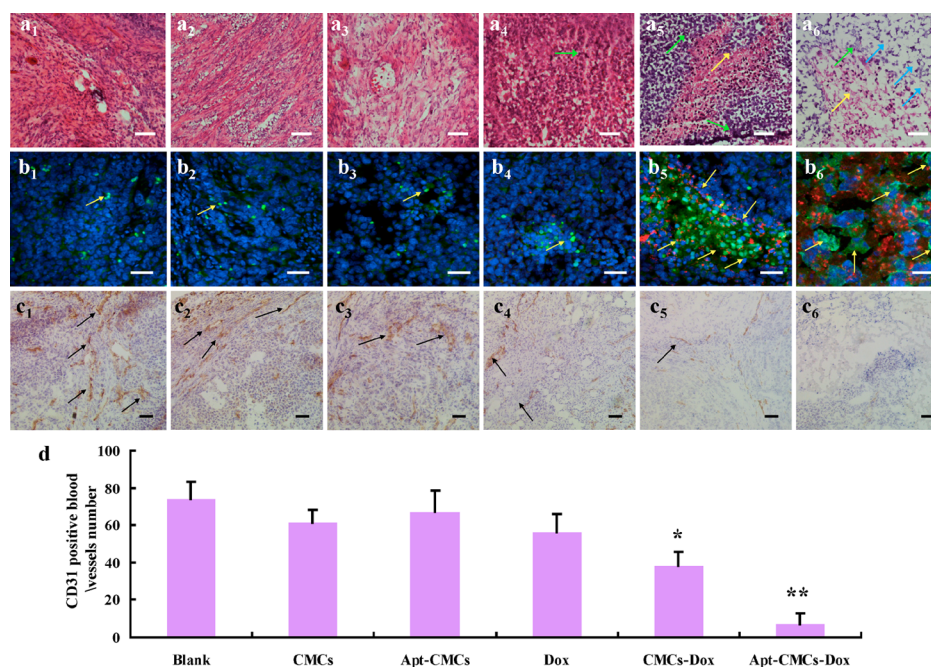
Figure 7. (a) Opitcal images of H&E stained tumors harvested from mice treated with different groups for 3 weeks: (1) saline, (2) CMCs, (3) Apt-CMCs, (4) free DOX, (5) CMCs/DOX and (6) Apt-CMCs/DOX groups, respectively. Yellow, green and blue arrows indicate the cytoplasm, cell nuclei and vacuoles in the tumors, respectively. (b) Fluorescent images of tumor apoptosis from different groups, respectively. Cell nuclei were stained with DAPI (blue) and DNA fragments were stained with TUNEL assay (green). DOX is visualized by its autofluorescence (red). (c) Optical images of immunohistological stained CD31 of tumor sections from mice treated with different groups for 3 weeks: (1) saline, (2) CMCs, (3) Apt-CMCs, (4) free DOX, (5) CMCs/DOX and (6) Apt-CMCs/DOX groups. Arrows indicate positive CD31 staining. (d) Number of CD31 positively stained blood vessels was calculated from each slide. The * and ** indicate significant differences at the $p < 0.05$ and $p < 0.01$ levels, respectively. Scale bar is 50 μm.

no indication of necrotic or apoptotic regions were observed in the saline, CMCs and Apt-CMCs groups. The cells were lightly stained by eosin, suggesting strong viability. In contrast, many cells in tumor tissue treated with free DOX were stained by eosin with obviously reduced cytoplasmic ratio (Figure 7a$_4$), suggesting the malfunction of cells. A lot of dark purple cell nuclei (Figure 7a$_5$, green arrows headed) were observed from the tumor treated with CMCs/DOX group, suggesting significant cell death and loss of cytoplasm (yellow arrows headed). Vacuoles were also observed in the tissues (blue arrows headed), which may be caused by the apoptosis of the cells inside the tumor. Significant cell necrosis and big vacuoles were observed full of the tumors from the Apt-CMCs/DOX group, indicating the necrosis of the tumors (Figure 7a$_6$).

DNA fragmentation in apoptosis is usually associated with ultrastructural changes in cellular morphology, which can be examined using the TUNEL assay. The *in situ* staining of DNA strand breaks detected by the TUNEL assay and subsequent visualization by fluorescent microscopy gives biologically significant data about DNA damage, as it is related to the apoptotic process. As shown in Figure 7b, the highest green fluorescent signal was detected from the Apt-CMCs/DOX group, indicating the most significant cell apoptosis. A certain amount of apoptotic signal was also observed from the CMCs/DOX group, but the intensity is much less than that of the Apt-CMCs/DOX group. In contrast, only a very limited amount of apoptotic signals were observed from free DOX group and other drug free control groups. It is worth noting that the strongest red fluorescent signal was observed within the tumor from the Apt-CMCs/DOX group, suggesting the highest DOX concentration inside tumors achieved by targeting vehicles. The

results agreed with that obtained from *in vivo* distribution study (Figure 5) and explained the highest tumor inhibition effect of the Apt-CMCs/DOX group. Very few DOX can be found in the free DOX group: this might be attributed to the rapid clearance of DOX by opsonization and uptake by the reticuloendothelial system.[36] It is also worth noting that a certain amount of DOX was found from CMCs/DOX group. This might be attributed to the longer retention time of DOX entrapped by the CMCs (Figure 5c) and thus increased possibility to reach tumor sites. Besides, it is still possible that a certain extent of CMCs reached tumors but is not visible in Figure 4 due to limited detection ability of *in vivo* fluorescent image assay.

Angiogenesis is a prerequisite for cancer survival, growth and metastasis. Therefore, CD31, an endothelial cell marker that is involved in new blood vessel formation, was investigated. An extensive brownish CD31 signal can be found in the tumors in saline, CMCs and Apt-CMCs groups (Figure 7c, arrows headed). The CD31 signal reduced significantly from the tumors of CMCs/DOX groups ($p < 0.05$, Figure 7d), suggesting the decrease of blood vessels. Almost no CD31 signal can be found in the tumors treated with Apt-CMCs/DOX, proving again the inhibition of tumor growth.

In summary, we have developed a robust and versatile system for *in vivo* drug delivery using CMCs, a mammal cell-derived microreservoir-type carrier. Unlike the traditional methods to generate cell ghosts, which requires complete or partial destruction of cells, CB is a drug that can reversibly destroy the cell skeleton at low dosages. The cells can recover after removal of CB and only a very few cells are dead during the process. As a result, the obtained CMCs maintain the important

membrane functions such as selective permeability and even the functions of built-in protein channels,[26] which are not possible for normal cell ghosts. CMCs are biocompatible, which was evident by the absence of cytotoxicity and inflammatory response *in vitro*, and the lack of weight loss and any abnormalities in the murine xenograft model, given repeated i.v. doses. We have also demonstrated that tumor targeting ligands, aptamer AS1411, can be linked to the surface of CMCs via the reaction with proteins on plasma membrane. This enables their specific targeting to some cancer cells, and triggers their rapid and efficient cell uptake. CMCs can package hydrophilic anticancer drug, contrast agent and macromolecules, i.e., doxorubicin, Gd-DTPA, and dextran respectively, despite their disparate structure, charge and size. Drug loading is easily carried out by permeabilizing the plasma membrane of CMCs with a specific surfactant, digitonin. The plasma membrane of CMCs can be resealed in the presence of Ca^{2+}. Thus, retention and sustained release of drug in CMCs *in vitro* and *in vivo*, after loading, can be achieved. Although the obvious accumulation is in major organs such as liver and lung, a significant portion of targeting CMCs can be accumulated in tumor tissue in the murine xenografts and thus deliver high concentration of drug into the tumor. As a result, Apt-CMCs/DOX can induce cell apoptosis, destroy blood vessels and finally inhibit tumor growth, with significantly reduced toxicity compared to free drug.

4. CONCLUSIONS

In this study, biocompatible cell membrane capsules were prepared from human endothelial cells with preserved membrane structure and functions. Cancer cell targeting aptamer AS1411 was conjugated onto the CMCs, which resulted in enhanced ingestion of CMCs in certain cancer cells and accumulation of CMCs in mouse tumor xenografts. Chemotherapeutics and contrast agents can be packaged into the CMCs by reversibly permeating their plasma membranes. The systematic administration of cancer targeting CMCs loaded with doxorubicin can inhibit tumor growth in mouse xenografts, with significantly reduced toxicity compared to free drug. These findings suggest that targeting CMCs may have considerable benefits in drug delivery and cancer treatment.

■ ASSOCIATED CONTENT

ⓈSupporting Information

The Supporting Information is available free of charge on the ACS Publications website at DOI: 10.1021/acsami.5b05065.

Additional characterizations data of the CMCs and Apt-CMCs (PDF).

■ AUTHOR INFORMATION

Corresponding Authors
*Jian-Qing Gao, Ph.D., Professor. Institute of Pharmaceutics, College of Pharmaceutical Sciences, Zhejiang University, 866# Yuhangtang Road, Hangzhou 310058, P.R. China. E-mail: gaojianqing@zju.edu.cn. Tel:+86-571-88208437.
*Zheng-Wei Mao, Ph.D., Associate Professor. MOE Key Laboratory of Macromolecular Synthesis and Functionalization, Department of Polymer Science and Engineering, Zhejiang University, 38# Zheda Road, Hangzhou 310027, P.R. China. E-mail: zwmao@zju.edu.cn. Tel: +86-571-87951922.

Author Contributions
§These authors contribute equally.

■ REFERENCES

(1) Langer, R. Drug Delivery and Targeting. *Nature* **1998**, *392*, 5−10.
(2) Brannon-Peppas, L.; Blanchette, J. Nanoparticle and Targeted Systems for Cancer Therapy. *Adv. Drug Delivery Rev.* **2012**, *64*, 206−212.
(3) Gao, J.; Lv, Q.; Li, L.; Tang, X.; Li, F.; Hu, Y.; Han, M. Glioma Targeting and Blood-Brain Barrier Penetration by Dual-targeting Doxorubincin Liposomes. *Biomaterials* **2013**, *34*, 5628−5639.
(4) Ferrari, M. Cancer Nanotechnology: Opportunities and Challenges. *Nat. Rev. Cancer* **2005**, *5*, 161−171.
(5) Murakami, M.; Cabral, H.; Matsumoto, Y.; Wu, S.; Kano, M.; Yamori, T.; Nishiyama, N.; Kataoka, K. Improving Drug Potency and Efficacy by Nanocarrier-mediated Subcellular Targeting. *Sci. Transl. Med.* **2011**, *3*, 64ra2.
(6) Georgieva, J.; Brinkhuis, R.; Stojanov, K.; Weijers, C.; Zuilhof, H.; Rutjes, F.; Hoekstra, D.; van Hest, J.; Zuhorn, I. Peptide-Mediated Blood-Brain Barrier Transport of Polymersomes. *Angew. Chem., Int. Ed.* **2012**, *51*, 8339−8342.
(7) Mundargi, R.; Babu, V.; Rangaswamy, V.; Patel, P.; Aminabhavi, T. Nano/micro Technologies for Delivering Macromolecular Therapeutics Using Poly(d,l-lactide-co-glycolide) and Its Derivatives. *J. Controlled Release* **2008**, *125*, 193−209.
(8) Li, N.; Peng, L.; Chen, X.; Zhang, T.; Shao, G.; Liang, W.; Gao, J. Antigen-loaded Nanocarriers Enhance the Migration of Stimulated Langerhans Cells to Draining Lymph Nodes and Induce Effective Transcutaneous Immunization. *Nanomedicine* **2014**, *10*, 215−223.
(9) Kotov, N. Inorganic Nanoparticles as Protein Mimics. *Science* **2010**, *330*, 188−189.
(10) Hyoudou, K.; Nishikawa, M.; Ikemura, M.; Kobayashi, Y.; Mendelsohn, A.; Miyazaki, N.; Tabata, Y.; Yamashita, F.; Hashida, M. Prevention of Pulmonary Metastasis From Subcutaneous Tumors by Binary System-based Sustained Delivery of Catalase. *J. Controlled Release* **2009**, *137*, 110−115.
(11) Hu, C.; Zhang, L.; Aryal, S.; Cheung, C.; Fang, R.; Zhang, L. Erythrocyte Membrane-Camouflaged Polymeric Nanoparticles as a Biomimetic Delivery Platform. *Proc. Natl. Acad. Sci. U. S. A.* **2011**, *108*, 10980−10985.
(12) Yoo, J.; Irvine, D.; Discher, D.; Mitragotri, S. Bio-inspired, Bioengineered and Biomimetic Drug Delivery Carriers. *Nat. Rev. Drug Discovery* **2011**, *10*, 521−535.
(13) Kriebardis, A.; Antonelou, M.; Stamoulis, K.; Economou-Petersen, E.; Margaritis, L.; Papassideri, I. Progressive Oxidation of Cytoskeletal Proteins and Accumulation of Denatured Hemoglobin in Stored Red Cells. *J. Cell. Mol. Med.* **2007**, *11*, 148−155.
(14) MacDiarmid, J.; Amaro-Mugridge, N.; Madrid-Weiss, J.; Sedliarou, I.; Wetzel, S.; Kochar, K.; Brahmbhatt, V.; Phillips, L.; Pattison, S.; Petti, C. Sequential Treatment of Drug-resistant Tumors with Targeted Minicells Containing siRNA or a Cytotoxic Drug. *Nat. Biotechnol.* **2009**, *27*, 643−651.
(15) MacDiarmid, J.; Amaro-Mugridge, N.; Madrid-Weiss, J.; Phillips, L.; Burn, A.; Paulin, R.; Haasdyk, J.; Dickson, K.; Brahmbhatt, V.; Pattison, S. Bacterially Derived 400 nm Particles for Encapsulation and Cancer Cell Targeting of Chemotherapeutics. *Cancer Cell* **2007**, *11*, 431−445.
(16) Noad, R.; Roy, P. Virus-like Particles as Immunogens. *Trends Microbiol.* **2003**, *11*, 438−444.

(17) Gao, J.; Eto, Y.; Yoshioka, Y.; Sekiguchi, F.; Kurachi, S.; Morishige, T.; Yao, X.; Watanabe, H.; Asavatanabodee, R.; Sakurai, F. Effective Tumor Targeted Gene Transfer Using PEGylated Adenovirus Vector via Systemic Administration. *J. Controlled Release* **2007**, *122*, 102−110.

(18) Ashley, C.; Carnes, E.; Phillips, G.; Padilla, D.; Durfee, P.; Brown, P.; Hanna, T.; Liu, J.; Phillips, B.; Carter, M. The Targeted Delivery of Multicomponent Cargos to Cancer Cells by Nanoporous Particle-supported Lipid Bilayers. *Nat. Mater.* **2011**, *10*, 389−397.

(19) Parodi, A.; Quattrocchi, N.; van de Ven, A.; Chiappini, C.; Evangelopoulos, M.; Martinez, J.; Brown, B.; Khaled, S.; Yazdi, I.; Enzo, M. Synthetic Nanoparticles Functionalized With Biomimetic Leukocyte Membranes Possess Cell-like Functions. *Nat. Nanotechnol.* **2013**, *8*, 61−68.

(20) Hu, C.; Fang, R.; Copp, J.; Luk, B.; Zhang, L. A Biomimetic Nanosponge That Absorbs Pore-forming Toxins. *Nat. Nanotechnol.* **2013**, *8*, 336−340.

(21) Hu, C.; Fang, R.; Luk, B.; Zhang, L. Nanoparticle-detained Toxins for Safe and Effective Vaccination. *Nat. Nanotechnol.* **2013**, *8*, 933−938.

(22) Théry, C.; Ostrowski, M.; Segura, E. Membrane Vesicles as Conveyors of Immune Responses. *Nat. Rev. Immunol.* **2009**, *9*, 581−593.

(23) Boilard, E.; Nigrovic, P.; Larabee, K.; Watts, G.; Coblyn, J.; Weinblatt, M.; Massarotti, E.; Remold-O'Donnell, E.; Farndale, R.; Ware, J. Platelets Amplify Inflammation in Arthritis via Collagen-dependent Microparticle Production. *Science* **2010**, *327*, 580−583.

(24) Tang, K.; Zhang, Y.; Zhang, H.; Xu, P.; Liu, J.; Ma, J.; Lv, M.; Li, D.; Katirai, F.; Shen, G. Delivery of Chemotherapeutic Drugs in Tumour Cell-derived Microparticles. *Nat. Commun.* **2012**, *3*, 1282.

(25) Pick, H.; Schmid, E.; Tairi, A.; Ilegems, E.; Hovius, R.; Vogel, H. Investigating Cellular Signaling Reactions in Single Attoliter Vesicles. *J. Am. Chem. Soc.* **2005**, *127*, 2908−2912.

(26) Mao, Z.; Cartier, R.; Hohl, A.; Farinacci, M.; Dorhoi, A.; Nguyen, T.; Mulvaney, P.; Ralston, J.; Kaufmann, S.; Möhwald, H. Cells as Factories for Humanized Encapsulation. *Nano Lett.* **2011**, *11*, 2152−2156.

(27) Zhang, T.; Huang, B.; Yuan, Z.; Hu, Y.; Tabata, Y.; Gao, J. Gene Recombinant Bone Marrow Mesenchymal Stem Cells as a Tumor-targeted Suicide Gene Delivery Vehicle in Pulmonary Metastasis Therapy Using Non-viral Transfection. *Nanomedicine* **2014**, *10*, 257−267.

(28) Han, M.; Lv, Q.; Tang, X.; Hu, Y.; Xu, D.; Li, F.; Liang, W.; Gao, J. Overcoming Drug Resistance of MCF-7/ADR Cells by Altering Intracellular Distribution of Doxorubicin via MVP Knock-down with a Novel siRNA Polyamidoamine-Hyaluronic acid Complex. *J. Controlled Release* **2012**, *163*, 136−144.

(29) Ireson, C.; Kelland, L. Discovery and Development of Anticancer Aptamers. *Mol. Cancer Ther.* **2006**, *5*, 2957−2962.

(30) Yu, D.; Zhang, Y.; Mao, Z.; Gao, C. Study of the Selective Uptake Progress of Aptamer-Modified PLGA Particles by Liver Cells. *Macromol. Biosci.* **2013**, *13*, 1413−1421.

(31) Eroglu, A.; Russo, M.; Bieganski, R.; Fowler, A.; Cheley, S.; Bayley, H.; Toner, M. Intracellular Trehalose Improves the Survival of Cryopreserved Mammalian Cells. *Nat. Biotechnol.* **2000**, *18*, 163−167.

(32) Walev, I.; Bhakdi, S.; Hofmann, F.; Djonder, N.; Valeva, A.; Aktories, K.; Bhakdi, S. Delivery of Proteins into Living Cells by Reversible Membrane Permeabilization with Streptolysin-O. *Proc. Natl. Acad. Sci. U. S. A.* **2001**, *98*, 3185−3190.

(33) Schulz, I. Permeabilizing Cells: Some Methods and Applications for the Study of Intracellular Processes. *Methods Enzymol.* **1990**, *192*, 280−300.

(34) Miyamoto, K.; Yamashita, T.; Tsukiyama, T.; Kitamura, N.; Minami, N.; Yamada, M.; Imai, H. Reversible Membrane Permeabilization of Mammalian Cells Treated with Digitonin and Its Use for Inducing Nuclear Reprogramming by Xenopus Egg Extracts. *Cloning Stem Cells* **2008**, *10*, 535−542.

(35) Niklas, J.; Melnyk, A.; Yuan, Y.; Heinzle, E. Selective Permeabilization for the High-throughput Measurement of Compart-mented Enzyme Activities in Mammalian Cells. *Anal. Biochem.* **2011**, *416*, 218−227.

(36) Nie, Y.; Ji, L.; Ding, H.; Xie, L.; Li, L.; He, B.; Wu, Y.; Gu, Z. Cholesterol Derivatives Based Charged Liposomes for Doxorubicin Delivery: Preparation, In Vitro and In Vivo Characterization. *Theranostics* **2012**, *2*, 1092−1103.

(37) Sy, J.; Seshadri, G.; Yang, S.; Brown, M.; Oh, T.; Dikalov, S.; Murthy, N.; Davis, M. Sustained Release of a p38 Inhibitor From Non-inflammatory Microspheres Inhibits Cardiac Dysfunction. *Nat. Mater.* **2008**, *7*, 863−868.

(38) Chatterjee, K.; Zhang, J.; Honbo, N.; Karliner, J. Doxorubicin Cardiomyopathy. *Cardiology* **2010**, *115*, 155−162.

(39) Shah, K. Mesenchymal Stem Cells Engineered for Cancer Therapy. *Adv. Drug Delivery Rev.* **2012**, *64*, 739−748.

(40) Hu, Y.; Fu, Y.; Tabata, Y.; Gao, J. Mesenchymal Stem Cells: a Promising Targeted-Delivery Vehicle in Cancer Gene Therapy. *J. Controlled Release* **2010**, *147*, 154−162.

(41) Wei, H.; Wu, A.; Hsu, C.; Lin, Y.; Cheng, W.; Su, C.; Chiu, W.; Whang-Peng, J.; Douglas, F.; Deng, W. The Development of a Novel Cancer Immunotherapeutic Platform Using Tumor-Targeting Mesen-chymal Stem Cells and a Protein Vaccine. *Mol. Ther.* **2011**, *19*, 2249−2257.

(42) Zischek, C.; Niess, H.; Ischenko, I.; Conrad, C.; Huss, R.; Jauch, K.; Nelson, P.; Bruns, C. Targeting Tumor Stroma Using Engineered Mesenchymal Stem Cells Reduces the Growth of Pancreatic Carcinoma. *Ann. Surg.* **2009**, *250*, 747−753.

(43) Meyerrose, T.; De Ugarte, D.; Hofling, A.; Herrbrich, P.; Cordonnier, T.; Shultz, L.; Eagon, J.; Wirthlin, L.; Sands, M.; Hedrick, M. In Vivo Distribution of Human Adipose-Derived Mesenchymal Stem Cells in Novel Xenotransplantation Models. *Stem Cells* **2007**, *25*, 220−227.